Quantifying Functional Group Compositions of Household Fuel Burning Emissions

Emily Y. Li[1], Amir Yazdani[2], Ann M. Dillner[3], Guofeng Shen[1], Wyatt M. Champion[4], James J. Jetter[1], William T. Preston[5], Lynn M. Russell[6], Michael D. Hays[1], and Satoshi Takahama[2]

[1]Air Methods and Characterization Division, U.S. Environmental Protection Agency, Office of Research and Development, Research Triangle Park, North Carolina 27709, USA
[2]Laboratory for Atmospheric Processes and their Impacts, École Polytechnique Fédérale de Lausanne, CH-1015 Lausanne, Switzerland
[3]Air Quality Research Center, University of California, Davis, Davis, CA 95616, USA
[4]Air Methods and Characterization Division, Oak Ridge Institute for Science and Education, U.S. Environmental Protection Agency, Office of Research and Development, Research Triangle Park, North Carolina 27709, USA
[5]CSS Inc., Durham, North Carolina 27713, United States
[6]Scripps Institution of Oceanography, University of California San Diego, La Jolla, California 92093, USA

Correspondence: Emily Li (li.emily@epa.gov) and Satoshi Takahama (satoshi.takahama@epfl.ch)

Abstract. Globally, billions of people burn fuels indoors for cooking and heating, which contributes to millions of chronic illnesses and premature deaths annually. Additionally, residential burning contributes significantly to black carbon emissions, which have the highest global warming impacts after carbon dioxide and methane. In this study, we use Fourier transform infrared spectroscopy (FTIR) to analyze fine particulate emissions collected on Teflon membrane filters from fifteen cookstove types and five fuel types. Emissions from three fuel types (charcoal, kerosene, and red oak wood) were found to have enough FTIR spectral response for functional group (FG) analysis. We present distinct spectral profiles for particulate emissions of these three fuel types. We highlight the influential FGs constituting organic carbon (OC) using a multivariate statistical method and show that OC estimates by collocated FTIR and thermal optical transmittance (TOT) are highly correlated, with a coefficient of determination of 82.5%. As FTIR analysis is fast, non-destructive, and provides complementary FG information, the analysis method demonstrated herein can substantially reduce the need for thermal-optical measurements for source emissions.

1 Introduction

Residential burning is a major source of organic carbon (OC), and contributes approximately 30% of global emissions of black carbon, which is estimated to have the third highest global warming impact after carbon dioxide and methane(Ramanathan et al., 2008; Bond et al., 2013). The World Health Organization (WHO) estimates that close to 4 million premature deaths per year are associated with exposure to household air pollution, mainly from solid-fuel burning(WHO, 2014; Lee et al., 2020). Recent studies have typically categorized fine particulate matter ($PM_{2.5}$) emissions from household fuel burn emissions by mass, OC, and elemental carbon (EC) emission factors using gravimetric and thermal-optical methods (e.g., IMPROVE and NIOSH protocols) (Roden et al., 2006; Sharma and Jain, 2019; Jetter et al., 2012). However, thermal-optical OC-EC

measurements can sometimes take more than 45 minutes per sample and are destructive, while providing limited information, as OC and EC alone are only bulk properties of carbonaceous particles.

In contrast to thermal-optical methods, Fourier transform infrared spectroscopy (FTIR) measurements take a few minutes per sample, are non-destructive and highly reproducible, and provide more chemical information. FTIR measurements have been shown to be in good agreement with common methods for chemical characterization of organic matter (OM) such as aerosol mass spectrometry (AMS) and thermal-optical analysis (Takahama et al., 2013; Dillner and Takahama, 2015; Reggente et al., 2016; Takahama et al., 2016b; Yazdani et al., 2021a, b; Boris et al., 2019). However, FTIR has not been extensively used for chemical analysis of primary particulate emissions from residential burning.

In the current study, we use FTIR to quantify the organic functional group (FG) composition of $PM_{2.5}$ emissions from cookstoves collected on polytetrafluoroethylene (PTFE) filters. We find that OC estimates from FTIR measurements and regression modeling are in good agreement with those from thermal optical transmittance (TOT). Our analysis highlights spectral differences among fuels (charcoal, kerosene, red oak wood, alcohol, and liquefied petroleum gas) and their particulate emissions during combustion. Estimates of aromatics and polycyclic aromatic hydrocarbons (PAHs) from FTIR measurements of particulate emissions from charcoal, kerosene, and red oak wood are compared with those using gas chromatography-mass spectrometry (GS-MS) measurements. Estimates of aromatics and PAHs from FTIR measurements have been previously unavailable for primary source emissions. Implications of this study include the widened and improved analytical-chemical portfolio for aerosol $PM_{2.5}$ emissions, leading to increased laboratory throughput and understanding of the compositional attributes of a known toxic $PM_{2.5}$ component.

2   Materials and Methods

An overview of cookstove testing, emissions sampling, OC-EC measurements, GC-MS PAH measurements, FTIR measurements, and post-processing are illustrated via flow chart in Fig. 1. Details of measurements and post-processing either described or cited from previous publications in the subsections below. In short, a range of stoves and fuels were tested for burn emissions, from which parallel PTFE membrane and quartz fiber (Qf) filter samples were collected. PTFE filters were used to measure gravimetric $PM_{2.5}$ mass, and then scanned using transmission-mode FTIR. The quartz filters were used to measure TOT OC-EC as well as GC-MS PAHs. From these sets of measurements, partial least squares regression (PLSR) models were built for the identification of important FTIR group frequencies for OC and PAH, and peak fitting and quantification of FGs, OC, and OM/OC were performed.

2.1   Cookstove emissions testing and sampling

Cookstove emissions tests were conducted at the U.S. Environmental Protection Agency cookstove test facility in Research Triangle Park, NC. Details of the facility and protocols are described in previous publications(Jetter and Kariher, 2009; Jetter et al., 2012; Shen et al., 2017a, b; Xie et al., 2018). We analyzed 152 samples from 15 different stoves and five fuel types,

50 pictured in Fig. 2. Fuels tested covered charcoal (56 samples), kerosene (21 samples), red oak wood (69 samples), alcohol (3 samples), and liquefied petroleum gas (LPG, 3 samples).

In this study, particulate emissions from stoves during the Water Boiling Test (WBT) were sampled. The WBT protocol (version 4, Global Alliance for Clean Cookstoves, 2014) includes three test phases: (1) a high-power cold-start (CS) phase in which the stove, pot, and water are at ambient temperature at the beginning of the test phase; (2) a high-power hot-start

55 (HS) in which the stove is hot at the beginning of the test phase; and (3) a low-power simmer phase (SIM) in which the water temperature is kept 3 °C below the boiling point (Sec. S1) (Jetter et al., 2012). A modified protocol described by Jetter et al. (2012) was used for the charcoal stove.

$PM_{2.5}$ was sampled isokinetically on Qf (47-mm diameter Tissuquartz™ pure quartz no binder, Pall Corporation) filters and PTFE membrane filters (47-mm diameter Teflo® membrane, Pall Corporation) positioned in parallel and downstream of $PM_{2.5}$

60 cyclones (URG; Chapel Hill, NC) at a flow rate of 16.7 liters per minute. $PM_{2.5}$ was also sampled downstream of the PTFE filter using a Qf back filter for artifact correction. The filter-based $PM_{2.5}$ sampling was conducted in a primary dilution tunnel for low-emission fuel-cookstove combinations (*e.g.*, forced-draft biomass stoves), and in a secondary dilution tunnel for those with high emissions (*e.g.*, natural-draft biomass stoves) to avoid overloading filters. After sampling, filters were stored in filter petri dishes at 253 K to minimize volatilization and chemical reactions.

65 ## 2.2 Measurements

From the PTFE and Qf filter samples collected, three quantitative measurements were obtained on all samples for use in FTIR post-processing: gravimetric $PM_{2.5}$ mass, TOT OC-EC measurements, and GC-MS PAH measurements. $PM_{2.5}$ mass was determined by weighing the PTFE filters (Pall Gelman) gravimetrically with a microbalance (MC5 Micro Balance, Sartorius) before and after sampling. FTIR spectra were gathered in transmission mode on the sampled PTFE filters. For FTIR analysis,

70 the mid-infrared spectra in the 4000–400 cm^{-1} range were obtained using a Bruker-Vertex 80 FTIR instrument equipped with an α deuterated lanthanum alanine doped triglycine sulfate (DLaTGS) detector, at a resolution of 4 cm^{-1}, in transmission mode, averaged over 64 scans.

OC and EC on Qf samples were measured using a thermal-optical transmittance instrument (TOT; Sunset Laboratory) and a revised NIOSH method 5040 (NIOSH, 1999). Blank PTFE and Qf filters were also collected at the cookstove test

75 facility and the associated $PM_{2.5}$ mass, OC, and EC backgrounds were measured and subtracted from test samples. In order to make measurements on Qf (EC, OC, GC-MS) and PTFE (FTIR, gravimetric) filters more comparable (i.e., to minimize the differences due to volatilization and adsorption artifacts for semivolatile aerosols), artifact correction was performed. For this purpose, the values measured on the Qf back filters were subtracted from those on the Qf samples in parallel to the PTFE filter.

Thermal extraction GC-MS (TEx-GC-MS) as described by Shen et al. (2017b) was used to identify and quantify individual

80 PAHs in sampled cookstove emissions for kerosene and red oak wood fuels. Briefly, a 0.4 cm^2 Qf punch (or three punches for artifact filters and low-emission samples from LPG) was placed inside a glass tube that was pre-baked to 550 °C and spiked with 1 μL of an internal standard mixture containing deuterated PAH compounds. Following automated tube insertion into the oven unit, the sample was heated to 325 °C at a rate of 50 °C/min and held for 11 min; 50 mL/min of helium (He) flowed

over the sample. Desorbate was directed to a cryogenically cooled programmable temperature vaporization inlet at -85 °C
operating in splitless mode. The GC inlet was rapidly heated at 720 °C/min to 325 °C. The sample was chromatographed
on an ultralow-bleed capillary column (DB-5, 30 m × 0.25 mm I.D. × 0.25 μm film thickness) with He as the carrier gas (1
mL/min). The GC oven was temperature-programmed as follows: 65 °C for 10 min ramped to 325 °C at a rate of 10 °C/min
and held for 15 min.

Chromatographed compounds (listed in Sec. S2) were detected using an Agilent 5973 MS detector operating in selected
ion monitoring mode. The internal standard method and a multilevel, linear ($R^2 > 0.9$) calibration was used (0.1–1 ng) for
PAH quantification. A mid-level calibration check was performed daily prior to sample analysis and was used as a continuing
calibration in cases where measured and fixed concentrations were not within 20%. Daily checks were within 20% for most
targets even when replicated over months. Mid-level check recoveries for PAHs were within $105\% \pm 33\%$ on average. PAHs
below their detection limit were reported as "ND". Retention time shifts were negligible ($< 1\%$) throughout the analysis.
Target analyte validation was achieved using the retention times and isotopic fragment ratios exceeding a 3:1 signal-noise
ratio. Carryover tests were performed by reheating the TEx sample/apparatus immediately following the initial extraction and
then examining the GC-MS chromatogram for the presence of target compounds, which indicated an extraction efficiency of
$> 98\%$. Naphthalene was the only PAH detected (0.16 ± 0.11 ng) above its method detection limit (0.02 ng) in the blank filters.
Similar to EC and OC, artifact correction was performed for PAHs by subtracting values of the quartz back filters from those
of the parallel filters.

2.3 Post-processing

The following subsections describe or cite from previous publications that describe the post-processing methods applied to
FTIR spectra to identify and quantify FGs.

2.3.1 Baseline correction and blank subtraction

The FTIR spectra were baseline-corrected using smoothing splines to exclude the contribution of light scattering by the PFTE
filter membrane and particles, and absorption by carbonaceous material (Kuzmiakova et al., 2016; Russo et al., 2014; Parks
et al., 2019). Graphitic carbon contributes to the mid-infrared spectra through electronic transition absorptions (Russo et al.,
2014; Parks et al., 2021). After eliminating the variability of FTIR baseline due to PTFE filter membrane, we regressed the
baseline value at 4000 cm^{-1} against EC and OC (major components of $PM_{2.5}$ in this study). A relatively large and statistically
significant coefficient for EC (2.2 times the coefficient of OC, $R^2 = 0.72$; Sec. S3) suggests that EC contributes significantly
to the FTIR baseline of combustion aerosols, and may be used for quantitative prediction of EC (Debus et al., 2021).

After baseline correction, a scaled version of the baseline-corrected blank filter spectrum was subtracted from the baseline-
corrected sample spectra (Yazdani et al., 2021b). This procedure allowed us to identify and quantify some organic FG absorp-
tions such as the out-of-plane (OOP) aromatic CH bands.

2.3.2 Quantification of functional groups

After determining the important FGs (by Variable Importance in Projection [VIP] scores method detailed in Secs. S4 and S5), their abundances were quantified using a multiple peak-fitting algorithm (Takahama et al., 2013; Reggente et al., 2019b). Aliphatic CH (aCH), aromatic CH (rCH), alcohol COH (aCOH), carboxylic acid (COOH), and non-acid carbonyl (naCO) groups were quantified in this work. OC concentrations and OM:OC ratios were then calculated using FG abundances with minimal assumptions about the number of carbon atoms attached to each FG (Takahama and Ruggeri, 2017).

For the calibration of aromatic CH groups using the OOP bending mode, we used the twelve samples of anthracene $C_{14}H_{10}$ analyzed by (Gilardoni et al., 2007) for the aromatic CH stretching mode. Anthracene powder (Sigma-Aldrich) was dissolved in high purity methanol (Fisher Scientific, Inc.), atomized with a constant output atomizer (TSI, Inc. model 3076) in nitrogen flow, and deposited on 37mm PTFE filters (Pall Gelman) restricted to a $1\,\mathrm{cm}$ diameter collection spot with a custom-made PTFE mask (Gilardoni et al., 2007). Areal mass loadings for these samples spanned a range between 26.8 and 1040 $\mu g\,cm^{-2}$. The spectra aquired by FTIR were pretreated according Sec. 2.3.1 and the bending mode peak near $750\,\mathrm{cm^{-1}}$ was used to build a calibration as described by Takahama et al. (2013) and Reggente et al. (2019a). In this case, the peak height is used rather than the peak area, and the calibration coefficient (interpreted as molar absorptivity) was estimated to be $0.017\,\mathrm{cm^2\,mol^{-1}}$ of CH bond with a fit of $R^2 = 0.93$. The mass loading of PAHs was estimated from the quantified bonds assuming an effective C/H molar ratio of 1.4 (similar to anthracene) to account for additional carbon atoms of PAHs associated with the measured aromatic CH bonds.

3 Results and Discussion

In the following sub sections, we first present overall OC, EC, and $PM_{2.5}$ measurements among different fuel types, test phases, and stoves. Thereafter, we present FTIR spectra of particulate emissions qualitatively as well as those of unburned fuels. TOT OC measurements are then combined statistically with the FTIR spectra to identify influential FGs for OC. Finally, influential FGs are quantified to estimate OC, OM, and OM/OC, as well as to compare with TOT OC and GC-MS PAH measurements.

3.1 OC, EC, and $PM_{2.5}$ emission factors

OC, EC, and $PM_{2.5}$ emission factors, expressed in grams of emission per MJ of energy delivered to the pot, are shown in Fig. 3. We observe a significant variation across red oak fueled stoves in terms of emission factors (Fig. 3). In particular, the 3-Stone Fire and the Envirofit G3300 stove (natural draft) have relatively high emission factors of OC and EC accompanied by lower modified combustion efficiencies (MCEs; Sec. S6). On the other hand, gasifier stoves such as EcoChula XXL have higher MCEs and around 10 times lower EC and OC emissions. Lower absorbances are also noticeable in the FTIR spectra of the EcoChula XXL stove especially in the CS and HS phases. OC and EC emission factors are slightly lower in the SIM phase compared to CS and HS phases. Nevertheless, the variations observed in the PM composition from red oak combustion across phases (characterized by elemental-carbon-to-total-carbon ratio, EC/TC, where TC = OC + EC) is not substantial when

compared to the variability in each phase (Fig. 3 and Fig. S4). The average EC/TC for red oak combustion aerosols is 0.58 ± 0.19. This value is on the higher end of those reported in previous studies on the emission factors of particles emitted from wood-burning cookstoves (0.07–0.64) (Roden et al., 2006; Novakov et al., 2000).

Variation in emission factors across phases is more significant for charcoal combustion emissions compared to other fuels.

150 The HS phase has the highest OC emission factor (Fig. 3). The EC emission factor and the EC/TC ratio increase significantly in the CS phase. The average EC/TC ratios of charcoal combustion aerosols for the CS phase and all phases combined are 0.78 ± 0.23 and 0.30 ± 0.40, respectively.

3.2 FTIR spectra and interpretation

Figure 4 exhibits distinct spectral profiles for $PM_{2.5}$ emitted from combustion of different fuel types. The FTIR spectra of

155 alcohol and LPG particulate emissions were omitted as they were noisy and had organic absorptions comparable to those of blank filters. This observation is corroborated by the negative or close-to-zero TOT OC measurements for alcohol and LPG emissions.

The spectra of red oak combustion aerosols display a strong and broad band at $3500 \ cm^{-1}$ related to aCOH across all phases. This group is abundant in wood constituents (lignin, cellulose, and hemicellulose). In addition, medium aCH absorbances at

160 3000–2800 cm^{-1}, medium carbonyl CO absorbances at around $1700 \ cm^{-1}$, and strong aromatic C=C absorbances at 1600 cm^{-1} are observed in the spectra of red oak combustion aerosols. The absorption band attributed to the lignin aromatic ring stretching vibration at $1515 \ cm^{-1}$ is also prominent in several spectra (Boeriu et al., 2004), consistent with the existence of aromatic compounds with similar structure to monolignols, which are found in plants. Aromatic CH OOP bands at around 750 cm^{-1} (Centrone et al., 2005) and occasionally aromatic stretching aCH bands at around $3050 \ cm^{-1}$ are also visible in the FTIR

165 spectra. The mean spectrum of the SIM phase has the weakest aromatic OOP band among all phases. Levoglucosan signatures described by Yazdani et al. (2021b) are observed in several spectra for all three phases. Inorganic nitrate absorbances at 1400 and 830 cm^{-1} are visible in some red oak samples especially in CS and HS phases.

The mid-infrared spectrum of unburned kerosene fuel (from Xia et al., 2017) displays strong aCH peaks and weak rCH stretching ($3050 \ cm^{-1}$) absorbances. This is consistent with kerosene fuel being predominantly composed of hydrocarbons,

170 the majority of which are straight-chain and cyclic with the rest being aromatic (Collins, 2007). An elemental analysis of unburned kerosene fuel (Sec. S7) also shows the insignificant contribution of elements other than H and C and a molar H/C ratio of about 2:1 suggesting long-chain or cyclic alkanes.

In contrast, aCH absorbances are much weaker in the particulate emissions of kerosene combustion in all three phases, with high CH_3/CH_2 peak ratios that indicate branched or small hydrocarbons. Furthermore, rCH absorptions are more prominent in

175 the particulate emissions, suggesting a significant formation of aromatic hydrocarbons and PAHs during the combustion. In the majority of spectra, moderate aCOH absorbances are observed. In several samples taken from the emissions of the kerosene wick-type cookstove, a sharp CO carbonyl peak at $1695 \ cm^{-1}$ is observed (Sec. S8). This peak is accompanied by a broad peak at 3400–2400 cm^{-1} (with doublets at 2600 and 2400 cm^{-1} attributed to the dimerized carboxylic acid OH), suggesting high

abstractandances of carboxylic acids (Pavia et al., 2008). The carbonyl peak with a relatively low frequency and the high abundance
of rCH indicate the existence of aromatic acids. Aromatic signatures appear to be more prominent in the CS and HS phases.

The charcoal spectrum (from Guo and Bustin, 1998) has weak aCH and carbonyl CO absorbances, and strong aromatic C=C
and aCOH absorbances. The weak aCH peaks are consistent with the low hydrogen content of the fuel (Sec. S7).However, the
mid-infrared spectra of particulate emissions from charcoal combustion show strong aCH peaks (Fig. 4). The aCH peaks are
especially prominent in the HS phase in which charcoal is added to the hot fuel bed (Fig. S1). In addition, the carbonyl CO
peak at 1700 cm^{-1} emerges in the charcoal combustion spectra in the HS phase, while being absent in the charcoal spectrum
itself. This observation suggests the formation of carbonyls during charcoal pyrolysis and burning. Charcoal combustion in the
cold start (CS) phase has the highest EC emission factor (Fig. 3), concurrent with prominent C=C absorbances at around 1600
cm^{-1} in the FTIR spectra. The ratio of the aromatic C=C peak (1600 cm^{-1}) to aromatic CH (750 cm^{-1}) is higher for charcoal
burning aerosols compared to other fuels, suggesting that aromatic compounds are poor in hydrogen (=C−H groups).

3.3   Quantified functional groups from FTIR spectra

The organic functional groups aliphatic CH (aCH), aromatic CH (rCH), alcohol COH (aCOH), carboxylic acid (COOH),
and non-acid carbonyl (naCO) groups were quantified by peak fitting to mid-infrared. The results of peak fitting are shown
in Fig. 5 in terms of OM emission factors and OM/OC ratios. OC estimated by FTIR from the abundances of FGs ("FG
OC") is highly correlated with TOT OC measurements ($R^2 = 0.83$; Fig. S12). However, FG OC underpredicts TOT OC by
around 40%, although artifact correction has been performed for TOT OC using Qf back filters. This underprediction can be
attributed to imperfect correction of quartz adsorption artifacts, volatilization of compounds from particles on PTFE filters
(Subramanian et al., 2004), uncharacterized FGs, uncertainties in FG absorption coefficients, underprediction of the fractional
carbon associated with each FG (Reggente et al., 2019a; Bürki et al., 2020). The operationally-defined EC and OC separation
threshold for TOT might also be another cause of this discrepancy (Chow et al., 2004). Nonetheless, the consistent mass
recovery permits us to make systematic comparisons regarding the OM composition using FG analysis.

The concentration of rCH was estimated in this work using the OOP band (750 cm^{-1}), which is more distinguishable than
the stretching mode vibration (3050 cm^{-1}) previously used. The OOP peak has a comparatively higher absorption coefficient
and does not overlap significantly with other group frequencies as does the stretching mode peak (e.g., with the ammonium
NH stretch). Peaks of the two vibrational modes exhibits a strong relationship (Fig. S9), but the OOP peak is expected to have
higher sensitivity due to the aforementioned reasons. Contrary to the peak at 3050 cm^{-1}, the peak at 1600 cm^{-1} attributed to
aromatic C=C is not highly correlated with the OOP peak (Fig. S10), especially for red oak burning aerosols — likely due to
high abundance of lignin pyrolysis products substituted rings. However, a qualitative relationship between rCH and TOT EC
concentrations, dependent on fuel type, can be observed (Fig. S11).

The estimates of rCH using this OOP bend are highly correlated ($R^2 = 0.84$; slope = 19.6) with the total PAH concentra-
tion by GC-MS measured for kerosene and red oak wood fuels (Fig. 6). The VIP scores of GC-MS total PAH concentration
regressed against mid-infrared absorbances also indicate the importance of the 750 cm^{-1} band for PAHs (Fig. 7). The magni-
tude of PAHs and aromatic estimated using this band is almost an order of magnitude higher than that measured by GC-MS

probably due to this band accounting for other unmeasured aromatic and PAH compounds. While our calibration for the total PAH is based on a single compound, variations in absorption coefficients on the order of 30% for the same FGs across different

215   compounds have been reported (Takahama et al., 2013; Reggente et al., 2019a). Furthermore, the C/H ratio assumed (1.4) for calculation of PAH concentrations by FTIR (Sec. 2.3.2) is a conservative one considering that the range of C/H values for compounds measured by GC-MS in this study was 1.0–2.0 (Sec. S2), and the highest abundance found for compounds with C/H greater than 1.44 (e.g., pyrene and fluoroanthene, benzo-a-pyrene). Adoption of higher values for this ratio leads to higher estimates of PAH, OM mass, and proportion of PAH in estimated OM; the value of this and the absorption coefficient can be

220   further constrained in future studies with additional experiments and inverse modeling approaches (e.g., Bürki et al., 2020). In summary, the apparent difference in magnitude of FTIR and GC-MS estimates of PAH abundance are beyond the levels of our anticipated uncertainty, and likely stems from the difference in approach between FG and molecular level analysis toward quantification of mass concentrations (Russell, 2003).

Summarizing the FTIR composition analysis, red oak combustion aerosols have the highest mean OM emissions factors

225   for all phases (Fig. 5), consistent with TOT OC measurements (Fig. 3). For all three phases, aCOH, aCH, and rCH groups constitute the majority of OM. Among different phases, the simmering (SIM) phase has a slightly lower OM emission. The rCH group abundance is significantly lower in the SIM phase. The lower concentration of this group in the SIM phase is also observed for other fuel types. This is also reflected in the higher OM/OC ratio of this phase compared to other phases. The average OM/OC ratio of red oak combustion aerosols is estimated to be around 1.7.

230   Kerosene combustion has the lowest average OM emissions factors compared to other fuels in all phases (Fig. 5; around 4 times lower than red oak). Interestingly, while kerosene OC and EC is not necessarily higher than others (Fig. 3), its proportion of aromatic CH (rCH) is higher (Fig. 5). No clear difference is observed between the mean OM emission factor among different phases. The rCH is estimated to be the most prominent FG for the kerosene burning aerosols followed in order by aCOH, aCH, and COOH. The average OM/OC ratio is 1.8 for the kerosene aerosols. Like red oak, the SIM phase has the highest OM/OC

235   ratio due to a higher abundance of COOH (more oxygenated) and lower abundance of rCH (likely due to more complete combustion).

Charcoal burning aerosols have average OM emission factors slightly lower than those of red oak combustion (Fig. 5). The aCH group is the most important FG for charcoal burning aerosols constituting up to 50% of OM. The aCOH and rCH are the most abundant groups after aCH. Other FGs exist in negligible amounts in charcoal burning aerosols. The average OM/OC

240   ratio for charcoal burning aerosols is 1.6, slightly lower than that of other fuels. Like other fuel types, the SIM phase has the highest OM/OC ratio and the lowest abundance of aromatics.

Previous studies correlate aromatics and PAHs with mutagenicity and carcinogenicity (Riedel et al., 2018; Shiraiwa et al., 2017; Gibbs-Flournoy et al., 2018; Mutlu Esra et al., 2016). Our analysis shows that these compounds are abundant even in relatively clean fuels (i.e., with low emission factors) like kerosene, which has a magnitude of emitted aerosol PAH as

245   high as charcoal, suggesting its harmfulness. This observation along with the highly oxygenated FGs present in kerosene OM is consistent with previous studies providing some evidence that kerosene emissions may impair lung function and increase infectious illness, asthma, and cancer risks (Lam et al., 2012).

4 Conclusions

This manuscript introduces FTIR as a measurement technique that can provide new insights into the organic composition of
aerosol emissions from cookstoves, in which variations in composition and overall emissions due to fuel type and operational
phase of the cookstove are evaluated. The FTIR analysis is applied directly to filters collected for gravimetric mass analysis and
does not require an additional sampling line. The OM composition in terms of oxygenated functional groups - carboxylic acids,
carbonyls, and alcohols - and PAHs vary substantially across fuel types, and in some cases, the operational phase of the stove.
Additionally, a qualitative comparison of emitted OM to the composition of the fuel is demonstrated through comparison of the
aerosol spectra to the spectra of the unburnt fuel. The overall organic carbon estimated by FTIR is approximately 60% of that
estimated by thermal optical transmittance, with an R^2 of 0.82. This mass recovery is on the low end of previously reported
OC and OM comparisons against thermal optical methods or aerosol mass spectrometry, and may indicate the additional
sampling artifacts in emissions studies, or the greater presence of carbon associated with uncharacterized functional groups
or skeletal carbon atoms that are missed by FTIR. A new development introduced in this manuscript is the quantification of
PAH concentrations — particularly important in fresh emissions — based on the OOP bending absorption peak of aromatics
by FTIR, which is more prominent than the stretching vibrations observed in the functional group region of the spectrum. The
estimate of PAH hydrocarbon mass loadings by FTIR is found to be five-fold greater than that the summed from 16 PAHs
analyzed by GC-MS, likely because FTIR estimates account for unmeasured PAH compounds in the samples. Thus, FTIR can
potentially provide an additional dimension of information for toxicity studies of emitted aerosols.

Author contributions. EYL, AMD, MDH, and ST conceived of the project and manuscript. GS performed the filter sample collection and
gravimetric analysis, WTP directed the OC-EC and PAH measurements and analysis, and EYL performed the FTIR measurements. EYL,
GS, WMC, JJJ, WTP, and ST contributed further data curation. AMD, JJJ, MDH, LMR, and ST provided resources and/or acquiring financial
support for the project. EYL, AY, and ST provided and implemented code and supporting algorithms and code components, and prepared data
visualization. EYL, AMD, MDH, and ST provided oversight and leadership responsibility for research planning and execution, including
mentorship. EYL, AY, WMC, MDH, and ST contributed to the initial draft, and all authors contributed to the review and editing of the written
manuscript.

Competing interests. The authors state no competing interests.

Disclaimer. The views expressed in this article/chapter are those of the authors and do not necessarily represent the views or policies of the
U.S. Environmental Protection Agency. Mention of trade names or commercial products does not constitute endorsement or recommendation
for use.

Acknowledgements. The authors thank the U.S. Environmental Protection Agency Office of Air Quality Planning and Standards for their administrative support, the Office of Research and Development for Quality Assurance support, and acknowledge funding from the Swiss National Science Foundation (200021_172923).

References

Boeriu, C. G., Bravo, D., Gosselink, R. J. A., and van Dam, J. E. G.: Characterisation of Structure-Dependent Functional Properties of Lignin with Infrared Spectroscopy, 20, 205–218, https://doi.org/10.1016/j.indcrop.2004.04.022, 2004.

Bond, T. C., Doherty, S. J., Fahey, D. W., Forster, P. M., Berntsen, T., Deangelo, B. J., Flanner, M. G., Ghan, S., Kärcher, B., Koch, D., Kinne, S., Kondo, Y., Quinn, P. K., Sarofim, M. C., Schultz, M. G., Schulz, M., Venkataraman, C., Zhang, H., Zhang, S., Bellouin, N., Guttikunda, S. K., Hopke, P. K., Jacobson, M. Z., Kaiser, J. W., Klimont, Z., Lohmann, U., Schwarz, J. P., Shindell, D., Storelvmo, T., Warren, S. G., and Zender, C. S.: Bounding the Role of Black Carbon in the Climate System: A Scientific Assessment, 118, 5380–5552, https://doi.org/10.1002/jgrd.50171, 2013.

Boris, A. J., Takahama, S., Weakley, A. T., Debus, B. M., Fredrickson, C. D., Esparza-Sanchez, M., Burki, C., Reggente, M., Shaw, S. L., Edgerton, E. S., and Dillner, A. M.: Quantifying Organic Matter and Functional Groups in Particulate Matter Filter Samples from the Southeastern United States – Part 1: Methods, 12, 5391–5415, https://doi.org/10.5194/amt-12-5391-2019, 2019.

Bürki, C., Reggente, M., Dillner, A. M., Hand, J. L., Shaw, S. L., and Takahama, S.: Analysis of Functional Groups in Atmospheric Aerosols by Infrared Spectroscopy: Method Development for Probabilistic Modeling of Organic Carbon and Organic Matter Concentrations, 13, 1517–1538, https://doi.org/10.5194/amt-13-1517-2020, 2020.

Centrone, A., Brambilla, L., Renouard, T., Gherghel, L., Mathis, C., Müllen, K., and Zerbi, G.: Structure of New Carbonaceous Materials: The Role of Vibrational Spectroscopy, 43, 1593–1609, https://doi.org/10.1016/j.carbon.2005.01.040, 2005.

Chong, I.-G. and Jun, C.-H.: Performance of Some Variable Selection Methods When Multicollinearity Is Present, 78, 103–112, https://doi.org/10.1016/j.chemolab.2004.12.011, 2005.

Chow, J. C., Watson, J. G., Chen, L.-W. A., Arnott, W. P., Moosmüller, H., and Fung, K.: Equivalence of Elemental Carbon by Thermal/Optical Reflectance and Transmittance with Different Temperature Protocols, 38, 4414–4422, https://doi.org/10.1021/es034936u, 2004.

Collins, C. D.: Implementing Phytoremediation of Petroleum Hydrocarbons, in: Phytoremediation: Methods and Reviews, edited by Willey, N., Methods in Biotechnology, pp. 99–108, Humana Press, https://doi.org/10.1007/978-1-59745-098-0_8, 2007.

Debus, B., Weakley, A. T., Takahama, S., George, K. M., Schichtel, B., Copeland, S., Wexler, A. S., and Dillner, A. M.: Quantification of major particulate matter species from a single filter type using infrared spectroscopy – Application to a large-scale monitoring network, preprint, Aerosols/Laboratory Measurement/Validation and Intercomparisons, https://doi.org/10.5194/amt-2021-382, 2021.

Dillner, A. M. and Takahama, S.: Predicting Ambient Aerosol Thermal-Optical Reflectance (TOR) Measurements from Infrared Spectra: Organic Carbon, 8, 1097–1109, https://doi.org/10.5194/amt-8-1097-2015, 2015.

Gibbs-Flournoy, E. A., Gilmour, M. I., Higuchi, M., Jetter, J., George, I., Copeland, L., Harrison, R., Moser, V. C., and Dye, J. A.: Differential Exposure and Acute Health Impacts of Inhaled Solid-Fuel Emissions from Rudimentary and Advanced Cookstoves in Female CD-1 Mice, 161, 35–48, https://doi.org/10.1016/j.envres.2017.10.043, 2018.

Gilardoni, S., Russell, L. M., Sorooshian, A., Flagan, R. C., Seinfeld, J. H., Bates, T. S., Quinn, P. K., Allan, J. D., Williams, B., Goldstein, A. H., Onasch, T. B., and Worsnop, D. R.: Regional Variation of Organic Functional Groups in Aerosol Particles on Four U.S. East Coast Platforms during the International Consortium for Atmospheric Research on Transport and Transformation 2004 Campaign, 112, https://doi.org/10.1029/2006JD007737, 2007.

Guo, Y. and Bustin, R. M.: FTIR Spectroscopy and Reflectance of Modern Charcoals and Fungal Decayed Woods: Implications for Studies of Inertinite in Coals, 37, 29–53, https://doi.org/10.1016/S0166-5162(98)00019-6, 1998.

315   Jetter, J., Zhao, Y., Smith, K. R., Khan, B., Yelverton, T., DeCarlo, P., and Hays, M. D.: Pollutant Emissions and Energy Efficiency under
Controlled Conditions for Household Biomass Cookstoves and Implications for Metrics Useful in Setting International Test Standards,
46, 10 827–10 834, https://doi.org/10.1021/es301693f, 2012.

Jetter, J. J. and Kariher, P.: Solid-Fuel Household Cook Stoves: Characterization of Performance and Emissions, 33, 294–305,
https://doi.org/10.1016/j.biombioe.2008.05.014, 2009.

320   Kuzmiakova, A., Dillner, A. M., and Takahama, S.: An Automated Baseline Correction Protocol for Infrared Spectra of Atmospheric Aerosols
Collected on Polytetrafluoroethylene (Teflon) Filters, 9, 2615–2631, https://doi.org/10.5194/amt-9-2615-2016, 2016.

Lam, N. L., Smith, K. R., Gauthier, A., and Bates, M. N.: Kerosene: A Review of Household Uses and Their Hazards in Low-and Middle-
Income Countries, 15, 396–432, https://doi.org/10.1080/10937404.2012.710134, 2012.

Lee, K. K., Bing, R., Kiang, J., Bashir, S., Spath, N., Stelzle, D., Mortimer, K., Bularga, A., Doudesis, D., Joshi, S. S., Strachan, F., Gumy,
325   S., Adair-Rohani, H., Attia, E. F., Chung, M. H., Miller, M. R., Newby, D. E., Mills, N. L., McAllister, D. A., and Shah, A. S. V.: Adverse
health effects associated with household air pollution: a systematic review, meta-analysis, and burden estimation study, The Lancet Global
Health, 8, e1427–e1434, https://doi.org/10.1016/S2214-109X(20)30343-0, 2020.

Mutlu Esra, Warren Sarah H., Ebersviller Seth M., Kooter Ingeborg M., Schmid Judith E., Dye Janice A., Linak William P., Gilmour M.
Ian, Jetter James J., Higuchi Mark, and DeMarini David M.: Mutagenicity and Pollutant Emission Factors of Solid-Fuel Cookstoves:
330   Comparison with Other Combustion Sources, 124, 974–982, https://doi.org/10.1289/ehp.1509852, 2016.

NIOSH: Elemental Carbon (Diesel Particulate): Method 5040, pp. 1–9, 1999.

Novakov, T., Andreae, M. O., Gabriel, R., Kirchstetter, T. W., Mayol-Bracero, O. L., and Ramanathan, V.: Origin of Carbonaceous Aerosols
over the Tropical Indian Ocean: Biomass Burning or Fossil Fuels?, 27, 4061–4064, https://doi.org/10.1029/2000GL011759, 2000.

Pandey, K. K.: A Study of Chemical Structure of Soft and Hardwood and Wood Polymers by FTIR Spectroscopy, Journal of Applied Polymer
335   Science, 71, 1969–1975, https://doi.org/10.1002/(SICI)1097-4628(19990321)71:12<1969::AID-APP6>3.0.CO;2-D, 1999.

Parks, D. A., Raj, K. V., Berry, C. A., Weakley, A. T., Griffiths, P. R., and Miller, A. L.: Towards a Field-Portable Real-Time Organic and
Elemental Carbon Monitor, 36, 765–772, https://doi.org/10.1007/s42461-019-0064-8, 2019.

Parks, D. A., Griffiths, P. R., Weakley, A. T., and Miller, A. L.: Quantifying Elemental and Organic Carbon in Diesel Particulate Matter by
Mid-Infrared Spectrometry, 0, 1–14, https://doi.org/10.1080/02786826.2021.1917764, 2021.

340   Pavia, D. L., Lampman, G. M., Kriz, G. S., and Vyvyan, J. A.: Introduction to Spectroscopy, Brooks Cole, 4 edn., 2008.

Ramanathan, V., Rodhe, H., Agrawal, M., Akimoto, H., Auffhammer, M., Chopra, U. K., Emberson, L., Hasnain, S. I., Iyngararasan, M.,
Jayaraman, A., Lawrence, M., Nakajima, T., Ruchirawat, M., Singh, A. K., Vincent, J. R., and Zhang, Y.: Atmospheric Brown Clouds:
Regional Assessment Report with Focus on Asia Summary, 2008.

Reggente, M., Dillner, A. M., and Takahama, S.: Predicting Ambient Aerosol Thermal-Optical Reflectance (TOR) Measurements from
345   Infrared Spectra: Extending the Predictions to Different Years and Different Sites, 9, 441–454, https://doi.org/10.5194/amt-9-441-2016,
2016.

Reggente, M., Dillner, A. M., and Takahama, S.: Analysis of Functional Groups in Atmospheric Aerosols by Infrared Spectroscopy: Sys-
tematic Intercomparison of Calibration Methods for US Measurement Network Samples, 12, 2287–2312, https://doi.org/10.5194/amt-12-
2287-2019, 2019a.

350   Reggente, M., Höhn, R., and Takahama, S.: An Open Platform for Aerosol InfraRed Spectroscopy Analysis – AIRSpec, 12, 2313–2329,
https://doi.org/10.5194/amt-12-2313-2019, 2019b.

Riedel, T. P., DeMarini, D. M., Zavala, J., Warren, S. H., Corse, E. W., Offenberg, J. H., Kleindienst, T. E., and Lewandowski, M.: Mutagenic Atmospheres Resulting from the Photooxidation of Aromatic Hydrocarbon and NOx Mixtures, 178, 164–172, https://doi.org/10.1016/j.atmosenv.2018.01.052, 2018.

355 Roden, C. A., Bond, T. C., Conway, S., and Pinel, A. B. O.: Emission Factors and Real-Time Optical Properties of Particles Emitted from Traditional Wood Burning Cookstoves, 40, 6750–6757, https://doi.org/10.1021/es052080i, 2006.

Russell, L. M.: Aerosol Organic-Mass-to-Organic-Carbon Ratio Measurements, 37, 2982–2987, https://doi.org/10.1021/es026123w, 2003.

Russo, C., Stanzione, F., Tregrossi, A., and Ciajolo, A.: Infrared Spectroscopy of Some Carbon-Based Materials Relevant in Combustion: Qualitative and Quantitative Analysis of Hydrogen, 74, 127–138, https://doi.org/10.1016/j.carbon.2014.03.014, 2014.

360 Sharma, D. and Jain, S.: Impact of Intervention of Biomass Cookstove Technologies and Kitchen Characteristics on Indoor Air Quality and Human Exposure in Rural Settings of India, 123, 240–255, https://doi.org/10.1016/j.envint.2018.11.059, 2019.

Shen, G., Gaddam, C. K., Ebersviller, S. M., Vander Wal, R. L., Williams, C., Faircloth, J. W., Jetter, J. J., and Hays, M. D.: A Laboratory Comparison of Emission Factors, Number Size Distributions, and Morphology of Ultrafine Particles from 11 Different Household Cookstove-Fuel Systems, 51, 6522–6532, https://doi.org/10.1021/acs.est.6b05928, 2017a.

365 Shen, G., Preston, W., Ebersviller, S. M., Williams, C., Faircloth, J. W., Jetter, J. J., and Hays, M. D.: Polycyclic Aromatic Hydrocarbons in Fine Particulate Matter Emitted from Burning Kerosene, Liquid Petroleum Gas, and Wood Fuels in Household Cookstoves, 31, 3081–3090, https://doi.org/10.1021/acs.energyfuels.6b02641, 2017b.

Shiraiwa, M., Ueda, K., Pozzer, A., Lammel, G., Kampf, C. J., Fushimi, A., Enami, S., Arangio, A. M., Fröhlich-Nowoisky, J., Fujitani, Y., Furuyama, A., Lakey, P. S. J., Lelieveld, J., Lucas, K., Morino, Y., Pöschl, U., Takahama, S., Takami, A., Tong, H., Weber, B., Yoshino,
370 A., and Sato, K.: Aerosol Health Effects from Molecular to Global Scales, 51, 13 545–13 567, https://doi.org/10.1021/acs.est.7b04417, 2017.

Subramanian, R., Khlystov, A. Y., Cabada, J. C., and Robinson, A. L.: Positive and Negative Artifacts in Particulate Organic Carbon Measurements with Denuded and Undenuded Sampler Configurations Special Issue of Aerosol Science and Technology on Findings from the Fine Particulate Matter Supersites Program, 38, 27–48, https://doi.org/10.1080/02786820390229354, 2004.

375 Takahama, S. and Ruggeri, G.: Technical Note: Relating Functional Group Measurements to Carbon Types for Improved Model-Measurement Comparisons of Organic Aerosol Composition, 17, 4433–4450, https://doi.org/10.5194/acp-17-4433-2017, 2017.

Takahama, S., Johnson, A., and Russell, L. M.: Quantification of Carboxylic and Carbonyl Functional Groups in Organic Aerosol Infrared Absorbance Spectra, 47, 310–325, https://doi.org/10.1080/02786826.2012.752065, 2013.

Takahama, S., Ruggeri, G., and Dillner, A. M.: Analysis of Functional Groups in Atmospheric Aerosols by Infrared Spectroscopy: Sparse
380 Methods for Statistical Selection of Relevant Absorption Bands, 9, 3429–3454, https://doi.org/10.5194/amt-9-3429-2016, 2016a.

Takahama, S., Ruggeri, G., and Dillner, A. M.: Analysis of Functional Groups in Atmospheric Aerosols by Infrared Spectroscopy: Sparse Methods for Statistical Selection of Relevant Absorption Bands, 9, 3429–3454, https://doi.org/10.5194/amt-9-3429-2016, 2016b.

WHO: Indoor Air Quality Guidelines: Household Fuel Combustion, pp. 1–172, http://www.who.int/iris/bitstream/10665/141496Summaryin6languages:http://apps.who.int/iris/handle/10665/144309/http://apps.who.int//iris/bitstream/10665/141496/1/
385 9789241548885_eng.pdf?ua=1, 2014.

Wold, S., Martens, H., and Wold, H.: The Multivariate Calibration Problem in Chemistry Solved by the PLS Method, in: Matrix Pencils, edited by Kågström, B. and Ruhe, A., Lect. Notes Math., pp. 286–293, Springer Berlin Heidelberg, 1983.

Wold, S., Johansson, E., and Cocchi, M.: 3D QSAR in Drug Design: Theory, Methods and Applications, pp. 523–550, 1993.

Xia, W., Zhou, C., and Peng, Y.: Improving Flotation Performance of Intruded Coal Using Heavy Oil as a Collector, 39, 1124–1130, https://doi.org/10.1080/15567036.2017.1299256, 2017.

Xie, M., Shen, G., Holder, A. L., Hays, M. D., and Jetter, J. J.: Light Absorption of Organic Carbon Emitted from Burning Wood, Charcoal, and Kerosene in Household Cookstoves, 240, 60–67, https://doi.org/10.1016/j.envpol.2018.04.085, 2018.

Yazdani, A., Dillner, A. M., and Takahama, S.: Estimating Mean Molecular Weight, Carbon Number, and OM/OC with Mid-Infrared Spectroscopy in Organic Particulate Matter Samples from a Monitoring Network, 14, 4805–4827, https://doi.org/10.5194/amt-14-4805-2021, 2021a.

Yazdani, A., Dudani, N., Takahama, S., Bertrand, A., Prévôt, A. S. H., El Haddad, I., and Dillner, A. M.: Characterization of Primary and Aged Wood Burning and Coal Combustion Organic Aerosols in Environmental Chamber and Its Implications for Atmospheric Aerosols, 21, 10 273–10 293, https://doi.org/10.5194/acp-21-10273-2021, 2021b.
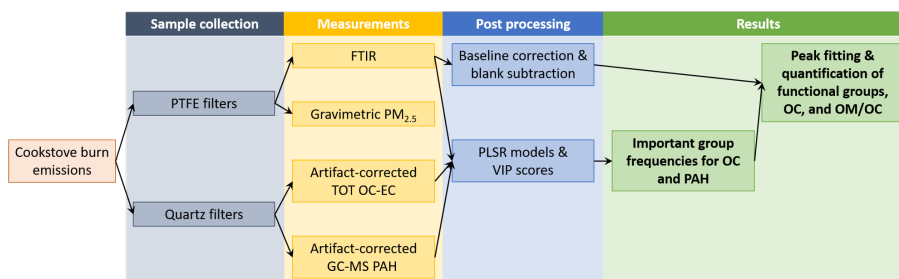
Figures

Figure 1. Flow chart from sample collection to measurements, post-processing, and results.

Figure 2. Photo showing 15 stoves used in this work. Charcoal stoves: (A) EcoZoom Jet, (B) Prakti Leo, (C) Envirofit CH4400, (D) Jiko Koa (inset), and (E) Éclair (inset). Kerosene stoves: (F) Model 2668 / Butterfly Wick and (G) Model 2412 / Butterfly Pressure. Red oak wood stoves: (H) Jiko Poa, (I) Envirofit G3300, (J) Philips HD4012, (K) Home Stove (Biolite), (L) EcoChula XXL (inset), and (M) 3-Stone Fire (inset). Alcohol stove: (N) CleanCook (inset). LPG stove: (O) Solgas.
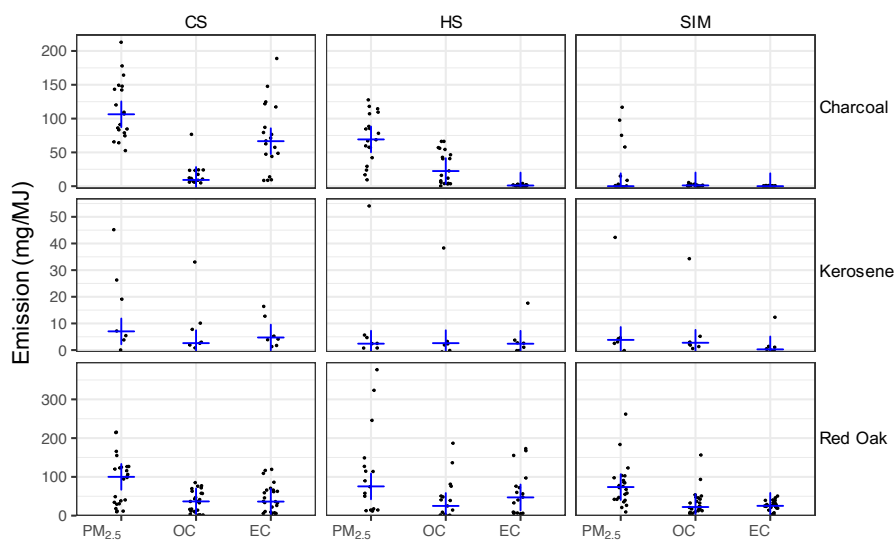
Figure 3. Emission factors (mg/MJ) of gravimetric PM$_{2.5}$ and artifact-corrected TOT OC and EC, separated by fuel type and test phase (CS: cold start, HS: hot start, SIM: simmering). Blue crosses show the median for each category.
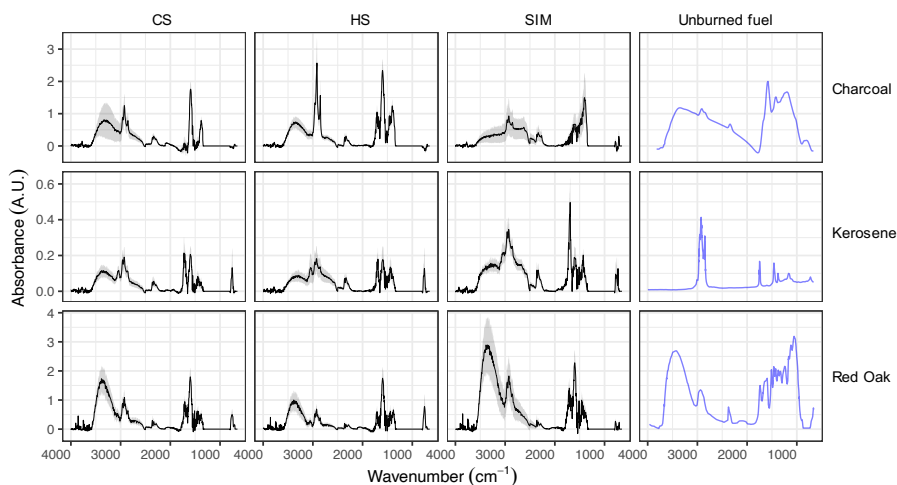
Figure 4. Average mid-infrared spectra of unburned fuels and their particulate emissions separated by source and test phase. Emission spectra are shown in terms of emission factors (absorbance divided by MJ energy delivered to the pot). Shaded bands show the mean spectrum $\pm$ 0.5 standard deviation. CS = cold start, HS = hot start, SIM = simmering. Features in the region between 1000–1300 cm^{-1}, which has interferences from PTFE filters, has been omitted. Spectra from unburned fuels (blue lines), presented with arbitrary scaling, are taken from the literature: Guo and Bustin (1998) for charcoal, Xia et al. (2017) for kerosene, and Pandey (1999) for red oak.
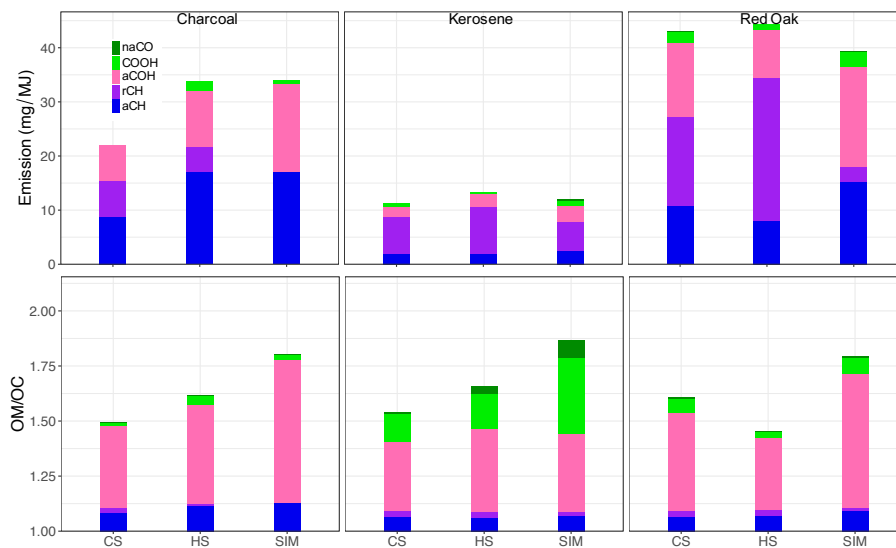
Figure 5. (Top row) OM emission factors calculated from mid-infrared spectroscopy, separated by functional group contribution, and averaged over each phase. (Bottom row) OM/OC ratios calculated from mid-infrared spectroscopy, separated by functional group contribution. CS = cold start, HS = hot start, SIM = simmering.
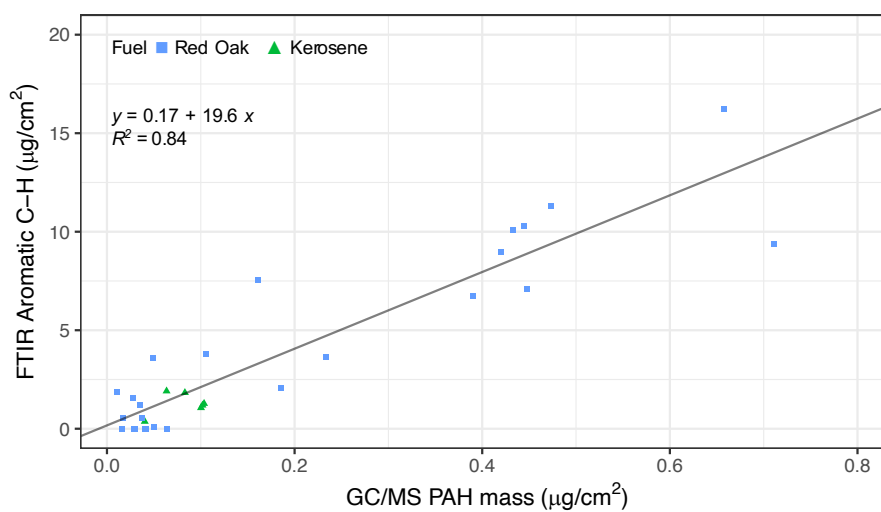
Figure 6. Scatter plot of aromatic CH concentration estimated using the peak at 750 cm^{-1} and GC-MS total PAH concentration.
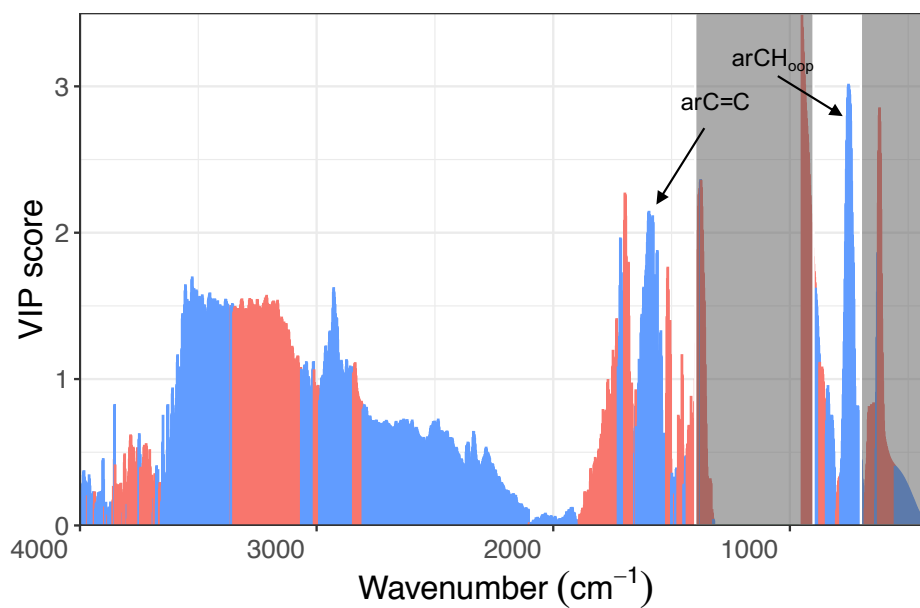
Figure 7. VIP scores of GC-MS sum of PAHs regressed against FTIR spectra.